Comparison of the generalized and bi-Maxwellian multimoment multispecies approaches of the terrestrial polar wind

François Leblanc, Daniel Hubert, Pierre-Louis Blelly

▶ **To cite this version:**

François Leblanc, Daniel Hubert, Pierre-Louis Blelly. Comparison of the generalized and bi-Maxwellian multimoment multispecies approaches of the terrestrial polar wind. Journal of Geophysical Research Space Physics, 2000, 105 (A2), pp.2551-2562. 10.1029/1999JA900474 . insu-02136149

HAL Id: insu-02136149

https://insu.hal.science/insu-02136149

Submitted on 21 May 2019

HAL is a multi-disciplinary open access archive for the deposit and dissemination of scientific research documents, whether they are published or not. The documents may come from teaching and research institutions in France or abroad, or from public or private research centers.

L'archive ouverte pluridisciplinaire **HAL**, est destinée au dépôt et à la diffusion de documents scientifiques de niveau recherche, publiés ou non, émanant des établissements d'enseignement et de recherche français ou étrangers, des laboratoires publics ou privés.

JOURNAL OF GEOPHYSICAL RESEARCH, VOL. 105, NO. A2, PAGES 2551-2562, FEBRUARY 1, 2000

Comparison of the generalized and bi-Maxwellian multimoment multispecies approaches of the terrestrial polar wind

François Leblanc[1] and Daniel Hubert

Département de Recherche Spatiale, Centre National de la Recherche Scientifique, Observatoire de Paris, Meudon, France

Pierre-Louis Blelly

Centre d'Etude Spatiale des Rayonnements, Toulouse, France

Abstract. A comparison between two multimoment approaches is provided in the context of an application to the terrestrial polar wind. We compare the bi-Maxwellian 16-moment approach with the 16-moment generalized model, which has been built in order to account for the suprathermal part of the velocity distribution function better than the previous multimoment approaches. This comparison has shown a general similarity between the two approaches and has shown that the better adapted closure assumption of the set of transport equations of the generalized model generates a higher acceleration. Moreover, the better determination of the collisional energy transfers generates a smaller increase of the temperature of the supersonic species that generally agrees with the adiabatic cooling assumption predicted by Monte Carlo or direct resolution of the Fokker Planck equation. The generalized model also provides the typical profiles of the velocity distribution function from the original collision-dominated region to the collisionless region. These profiles are in good agreement with the Monte Carlo and collision kinetic resolution in the collision-dominated region and in the lower part of the transition region.

1. Introduction

The terrestrial polar wind is a flow composed mainly of O^+ ions, H^+ ions, and electrons escaping from the terrestrial polar regions along the opened magnetic field lines. Its description all along its expansion is a difficult task since it goes through different states: from subsonic regime to supersonic regime, from state chemically dominated to diffusive state, and from collision-dominated regions to collisionless regions. This last characteristic, in particular, cannot be well described by the classical approaches: the hydrodynamic approaches are only well adapted to collision-dominated regions, whereas the exospheric approaches are only well adapted to collisionless regions.

Therefore, since the first hydrodynamic approach proposed by *Banks and Holzer* [1968], several different approaches to the terrestrial polar wind have been developed. A method issued from the theoretical approach of *Grad* [1958] and usually named the multimoment approach has been developed by *Demars and Schunk* [1979] and is often used in applications to the expansion of the terrestrial polar wind [*Blelly and Schunk*, 1993]. Recently, the Monte Carlo approach of *Barghouthi et al.* [1993] and of *Barakat et al.* [1995] has provided new behaviors of the velocity distribution function in the transition region and has enhanced the importance of this region in the expansion of the polar wind. A kinetic approach, which directly solved the linearized Fokker Planck equation, has been recently applied [*Lie-Svendsen and Rees*, 1996; *Pierrard and Lemaire*, 1998] from the collision-dominated region to the collisionless region through a transition region.

The great interests of a multimoment multispecies approach with respect to the fluid approach or direct resolution of the Fokker Planck equation include the following.

1. The species are described with the same model (contrary to the semikinetic approach, for example).

2. The model is self-consistent: all the types of collisions and particularly the collision between particles of

[1]Now at Department of Astronomy, University of Virginia, Charlottesville.

Copyright 2000 by the American Geophysical Union.

Paper number 1999JA900474.
0148-0227/00/1999JA900474$09.00

the same species are considered, contrary to the present status of the Monte Carlo and collision kinetic methods.

3. The lower boundary condition is defined in a collision-dominated region and then corresponds to the well-known thermodynamic equilibrium state.

4. The treatment of the heat flow is made from the collision-dominated region to the collisionless region with no assumption of a baropause or an exobase as in the kinetic collisionless approach. It is made through an equation that gives the spatial and temporal evolution of the heat flow and not through the classical conductivity thermal relation.

5. The major difficulty of such an approach is the necessity to determine high-order velocity moments, which implies lengthy calculations and the resolution of a large set of transport equations.

In this paper we compare the generalized 16-moment model [*Leblanc and Hubert*, 1997, 1998, 1999; *Leblanc et al.*, 2000] with the 16-moment bi-Maxwellian model of *Blelly and Schunk* [1993]. The generalized model was developed in order to take into account the contribution of the suprathermal part of the velocity distribution function better than it had been accounted for in the previous multimoment approaches. Indeed, above the collision-dominated region all the applications to the terrestrial polar wind agree to predict non-Maxwellian features of the distribution. *Leblanc and Hubert* [1997, 1998] underlined that in such conditions the bi-Maxwellian approach presents some problems. The predicted distribution function has negative values [*Leblanc and Hubert*, 1997], and the associated set of transport equations is no more valid according to the hyperbolicity and realizability criteria [*Leblanc and Hubert*, 1998]. On the contrary, the new closure assumption associated with the generalized multimoment set of transport equations is in better agreement with these non-Maxwellian features since the suprathermal particles have an explicit contribution to the heat flow equation. The velocity distribution function does not display negative values [*Leblanc and Hubert*, 1997], and the set of transport equations is well constructed [*Leblanc and Hubert*, 1998]. Moreover, *Leblanc et al.* [2000] showed that the collisional transfers associated with the generalized approach provide new contributions that could significantly change the transfers of impulsion and energy between species.

In section 2 the set of transport equations of the generalized model and the considered application are presented. In section 3, two comparisons between generalized and bi-Maxwellian approaches are provided. In section 4, we briefly compare the generalized solution with the solution obtained by other approaches to the terrestrial polar wind. Section 5 is a conclusion.

2. Application of the Generalized Model to the Terrestrial Polar Wind

In this section we present the generalized model [*Leblanc and Hubert*, 1997, 1998, 1999; *Leblanc et al.*, 2000] in the context of an application to the terrestrial polar wind derived from *Blelly and Schunk* [1993].

1. We consider the motion of three interacting species, H^+ ions, O^+ ions, and electrons, which interact with each other and, in the ionosphere, with a background of neutrals composed of H, O, O_2, and N_2.

2. The motion of the charged particles is supposed to be confined along the magnetic field lines. The description of the characteristics for each of the different charged species is then reduced to six independent parameters: the density n_s, the mean velocity u_s, parallel and perpendicular temperatures $T_{s\parallel}$ and $T_{s\perp}$, a heat flow for parallel energy $q_s{}^{\parallel}$, and a heat flow for perpendicular energy $q_s{}^{\perp}$ (for a complete definition of these parameters, see *Leblanc et al.* [2000]). The subscript or superscript $\parallel$ and $\perp$ refer to the parallel and perpendicular directions to the magnetic field, respectively. The configuration of the magnetic field is supposed to be fixed with respect to the motion of the particles, and the section of a magnetic field tube is supposed to diverge following a r^{-3} law, where r is the geocentric distance.

3. The collisions between charged particles are Coulomb collisions. The nonresonant ion neutral interactions are approximated by a Maxwell molecule interaction potential with an appropriate collision frequency as described by *Demars and Schunk* [1979].

4. We consider, as did *Blelly and Schunk* [1993], the production rate of H^+ to be due to the charge exchange reaction $H + O^+ \rightarrow H^+ + O$ and the loss rate to be due to the reverse reaction. We also introduce a production rate of O^+ ions composed of a solar photoionization and of a charge exchange reaction that is the reverse of the previous reaction. A loss rate of O^+ is also taken into account because of the charge exchange reaction associated with the previous reaction and because of chemical reactions with the O_2 and N_2 neutrals.

The generalized set of transport equations for the six velocity moments of the species s follows.

Number density equation

$$\frac{\partial n_s}{\partial t} + u_s \frac{\partial n_s}{\partial r} + n_s \frac{\partial u_s}{\partial r} + \frac{n_s u_s}{A} \frac{\partial A}{\partial r} = \frac{\delta n_s}{\delta t}, \qquad (1)$$

Momentum equation

$$\frac{\partial u_s}{\partial t} + u_s \frac{\partial u_s}{\partial r} + \frac{k_B T_{s\parallel}}{\rho_s} \frac{\partial n_s}{\partial r} + \frac{k_B}{m_s} \frac{\partial T_{s\parallel}}{\partial r} + \frac{k_B (T_{s\parallel} - T_{s\perp})}{m_s} \frac{1}{A} \frac{\partial A}{\partial r} - \frac{e_s}{m_s} E - G = \frac{\delta u_s}{\delta t}, \qquad (2)$$

Parallel temperature equation

$$\frac{\partial T_{s\parallel}}{\partial t} + u_s \frac{\partial T_{s\parallel}}{\partial r} + 2T_{s\parallel} \frac{\partial u_s}{\partial r} + \frac{1}{n_s k_B} \frac{\partial q_s{}^{\parallel}}{\partial r} + \frac{q_s{}^{\parallel} - 2q_s{}^{\perp}}{n_s k_B} \frac{1}{A} \frac{\partial A}{\partial r} = \frac{1}{n_s k_B} \frac{\delta T_{s\parallel}}{\delta t}, \qquad (3)$$

Perpendicular temperature equation

$$\frac{\partial T_{s\perp}}{\partial t} + u_s \frac{\partial T_{s\perp}}{\partial r} + \frac{1}{n_s k_B} \frac{\partial q_s{}^{\perp}}{\partial r} + \left(\frac{2q_s{}^{\perp}}{n_s k_B} + u_s T_{s\perp}\right) \frac{1}{A} \frac{\partial A}{\partial r} = \frac{1}{n_s k_B} \frac{\delta T_{s\perp}}{\delta t}, \quad (4)$$

Parallel heat flow equation

$$\frac{\partial q_s{}^{\parallel}}{\partial t} - \frac{m_s}{2^{1/3}} \left(\frac{q_s{}^{\parallel}}{\rho_s}\right)^{4/3} \frac{\partial n_s}{\partial r} + \frac{3 n_s k_B{}^2 T_{s\parallel}}{m_s} \frac{\partial T_{s\parallel}}{\partial r} + 4 q_s{}^{\parallel} \frac{\partial u_s}{\partial r} + \left[u_s + 2^{5/3} \left(\frac{q_s{}^{\parallel}}{\rho_s}\right)^{1/3}\right] \frac{\partial q_s{}^{\parallel}}{\partial r} + u_s q_s{}^{\parallel} \frac{1}{A} \frac{\partial A}{\partial r} + \left[6 n_s m_s \left(\frac{q_s{}^{\parallel}}{2 n_s m_s}\right)^{4/3} - 3 \frac{q_s{}^{\parallel} q_s{}^{\perp}}{n_s k_B T_{s\parallel}}\right] \frac{1}{A} \frac{\partial A}{\partial r} = \frac{\delta q_s{}^{\parallel}}{\delta t} - 3 n_s k_B T_{s\parallel} \frac{\delta u_s}{\delta t}, \quad (5)$$

Perpendicular heat flow equation

$$\frac{\partial q_s{}^{\perp}}{\partial t} - \frac{q_s{}^{\parallel} q_s{}^{\perp}}{n_s{}^2 k_B T_{s\parallel}} \frac{\partial n_s}{\partial r} + 2 q_s{}^{\perp} \frac{\partial u_s}{\partial r} + \frac{n_s k_B{}^2 T_{s\parallel}}{m_s} \frac{\partial T_{s\perp}}{\partial r} - \frac{q_s{}^{\parallel} q_s{}^{\perp}}{n_s k_B T_{s\parallel}{}^2} \frac{\partial T_{s\parallel}}{\partial r} + \left(u_s + \frac{q_s{}^{\parallel}}{n_s k_B T_{s\parallel}}\right) \frac{\partial q_s{}^{\perp}}{\partial r} + \frac{q_s{}^{\perp}}{n_s k_B T_{s\parallel}} \frac{\partial q_s{}^{\parallel}}{\partial r} + \left[\frac{n_s k_B^2 T_{s\perp}}{m_s} (T_{s\parallel} - T_{s\perp}) + 2 u_s q_s{}^{\perp}\right] \frac{1}{A} \frac{\partial A}{\partial r} + 2 \frac{q_s{}^{\parallel} q_s{}^{\perp}}{n_s k_B T_{s\parallel}} \frac{1}{A} \frac{\partial A}{\partial r} = \frac{\delta q_s{}^{\perp}}{\delta t} - n_s k_B T_{s\perp} \frac{\delta u_s}{\delta t}. \quad (6)$$

A is the section of the magnetic flux tube at the geocentric distance r. It is related to the magnetic field strength B by the Maxwell law $\partial[A(r)B(r)]/\partial r = 0$, which expresses the conservation of the magnetic flux. G is the acceleration due to gravitation, and E is the charge separation electrostatic field. Here k_B is the Boltzmann constant; $\rho_s = n_s m_s$ the mass density; and e_s the electric charge.

The terms $\frac{\delta n_s}{\delta t}$, $\frac{\delta u_s}{\delta t}$, $\frac{\delta T_{s\parallel}}{\delta t}$, $\frac{\delta T_{s\perp}}{\delta t}$, $\frac{\delta q_s{}^{\parallel}}{\delta t}$, and $\frac{\delta q_s{}^{\perp}}{\delta t}$ are the collisional transfers between the s species and the t species. These terms introduce all the chemical and photoionization effects. They have been presented by *Leblanc et al.* [2000] and are determined by a two-dimensional (2-D) numerical integration. These integrals are easily and accurately determined by numerical methods using an adapted Romberg's extrapolation method [*Press et al.*, 1989]. However, this method needs too much time of integration in the context of a resolution of (1)-(6). As a matter of fact, for a complete resolution of the generalized model in the terrestrial polar wind we need to calculate this 2-D integral a number of times equal to 6 (number of velocity moment equations) × 3 (number of charged species) × 3 (number of species that interact with one species) × 70 (number of steps in altitude in a range 200-4000 km) × 12 × 3600 (number of steps of 1 s in 12 hours of simulation time), which is $\sim 10^9$. This very large number eliminates any method of determination of the collisional transfer that could not be based on analytic formulations of the collisional transfers. Therefore we have chosen to replace the generalized collisional transfers by the analytic expressions determined for the 16-moment bi-Maxwellian approach [*Chodura and Pohl*, 1971]. Indeed, *Leblanc et al.* [2000] show that the *Chodura and Pohl* [1971] expressions are more complete and that they approximate more accurately the exact generalized collisional transfers than the expressions of *Blelly and Schunk* [1993]. The method to solve the set of transport equations is the same as is given by *Blelly and Schunk* [1993] and is based on the flux-corrected transport technique [*Boris*, 1976]. All the solutions shown in this paper are stationary solutions.

The following boundary conditions are used in this application.

1. The heat flow and the velocity of the O^+ ions are set to be positive at the top boundary in order to impose an upward flow. We impose a Mach number for the O^+ ion velocity equal to 0.3, where the Mach number is defined as $M_{O^+} = u_{O^+}/v_{thO^+}$ with $v_{thO^+} = (k_B T_{O^+\parallel}/m_{O^+})^{1/2}$.

2. We restrain our application to altitudes in a range from 200 to 4000 km in order to be able to compare our results with the in situ measurements [*Chandler et al.*, 1991; *Abe et al.*, 1993].

3. At the lower boundary the characteristics of the charged particles are defined by the interaction with the neutrals. The neutral atmosphere is described by the Mass Spectrometer Incoherent Scatter 1986 model (MSIS-86) atmospheric model [*Hedin et al.*, 1987]. The model of photoionization that we use in our simulation corresponds to high latitudes summertime sunlit ionosphere.

4. Electron heating from the magnetosphere is taken into account by a downward electron heat flow at the top boundary of -2.5×10^{-3} erg cm^{-2}s^{-1}.

For a summertime sunlit and high-latitude ionosphere the typical in situ measurements of the H^+ density are 100 cm^{-3} at 2000 km in altitude and 30 cm^{-3} at 4000 km [*Chandler et al.*, 1991]. For the O^+ ions the density evolves from 2000 cm^{-3} at 2000 km to 700 cm^{-3} at 4000 km [*Chandler et al.*, 1991]. The velocity of the H^+ ions is 1 km s^{-1} at 2000 km and 6 km s^{-1} at 4000 km in altitude [*Abe et al.*, 1993]. For the O^+ ions the velocity is close to zero but should be positive at 4000 km in altitude [*Abe et al.*, 1993], which is in good agreement with the boundary condition on u_{O^+} at 4000 km. The ion temperature is in the range 3000-7000 K [*Ganguli*, 1996]. The electron temperature should be ~4000 K at

2000 km in altitude and 8000 K at 4000 km [*Oyama and Abe*, 1995].

3. Comparison Between the Generalized and Bi-Maxwellian Models

3.1. Role of the New Closure Assumption

Leblanc and Hubert [1997] underlined that the limitation of a multimoment approach derives from the necessity to define a closure assumption for the set of transport equations. In (5) and (6) this requirement appears through the dependence of the velocity moments $< c_{\parallel}^4 >$ and $< c_{\perp}^4 >$ with respect to the lower-order velocity moments $(< c_{\parallel}^2 >)^2$ and $(< c_{\parallel}^3 >)^{4/3}$, relations which have been determined by *Leblanc and Hubert* [1998]. As an example, this change generates a new thermal conductivity law associated with the generalized model. This section presents some of the properties provided by this new closure assumption.

Figure 1 provides the H^+ macroscopic parameters determined by two different multimoment approaches in the context of the application described in section 2. We only present the H^+ ion parameters because the differences are less significant for the O^+ ions and the electrons. One of the models (solid line) is the 16-moment generalized model where the collisional transfers are approximated by the collisional transfers of *Blelly and Schunk* [1993]. The other model (dotted line) is the complete 16-moment bi-Maxwellian approach defined by *Blelly and Schunk* [1993]. The differences between these two models then reduce to the transport part of the heat flow equations, i.e., the left side of (5) and (6).

Some discrepancies are found around 1000 km, where the diffusion effects become higher than the ion/neutral collision effects. The first consequence of the new closure assumption is that the maximum value of the parallel heat flow $q^{\parallel}$ around 2000 km (Figure 1f) is smaller in the generalized solution than in the bi-Maxwellian one. From 2000 to 4000 km in altitude this parameter tends rapidly to zero according to the solution obtained with the bi-Maxwellian model, whereas the generalized parallel heat flow at 4000 km is still important with respect to its maximum value. This discrepancy could be explained by the fact that in the generalized model the heat flow is not only related to the gradient of temperature but, according to (5), also to the gradient of density. Whereas the increase of the parallel temperature is less important in the generalized model above 2000 km compared to the solution of the

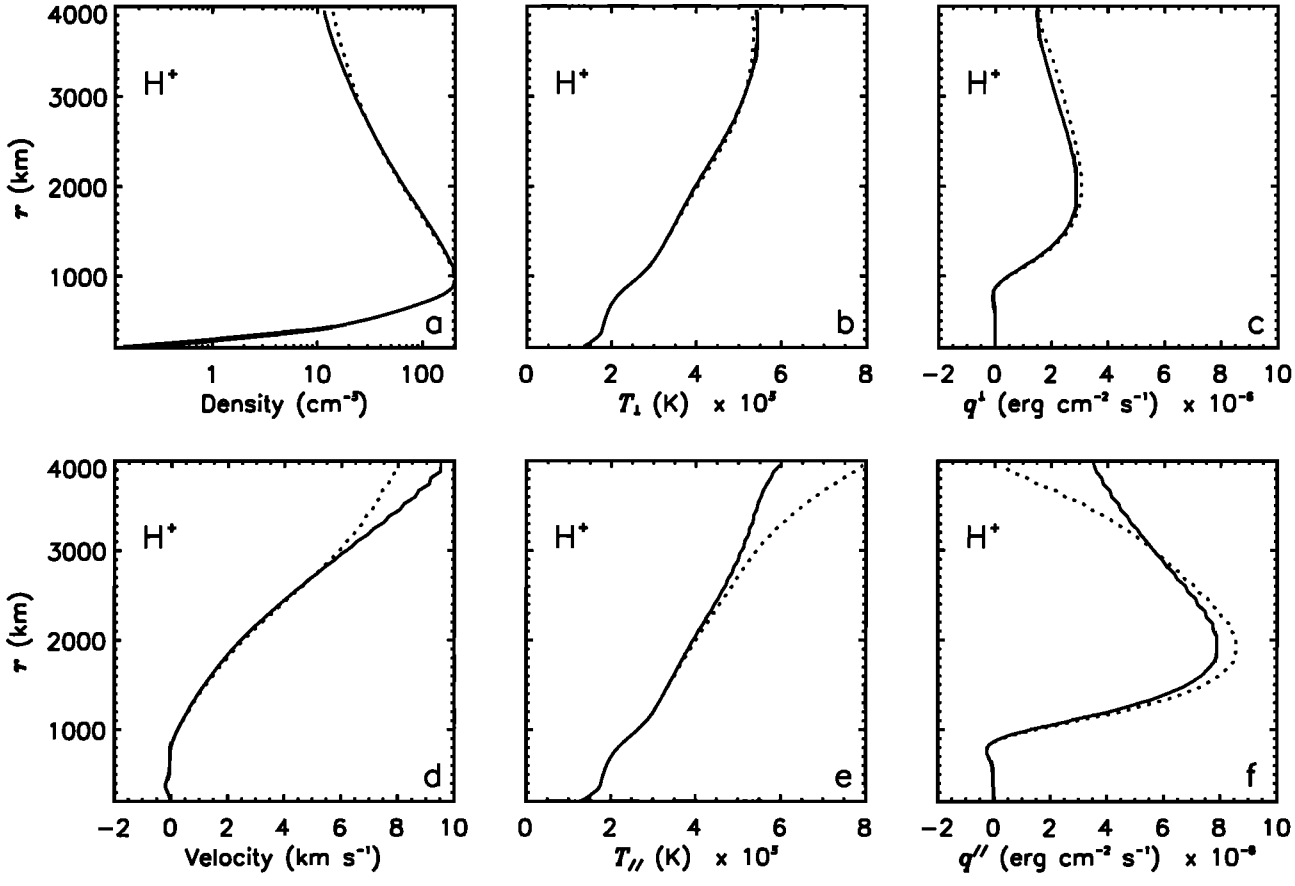

Figure 1. Macroscopic parameters derived from the modified generalized model (solid line) as decribed in section 3.1 and from the bi-Maxwellian model (dotted line): (a) H^+ ion density, (b) H^+ ion perpendicular temperature, (c) H^+ ion heat flow of perpendicular energy, and (d) H^+ ion velocity, (e) H^+ ion parallel temperature, (f) H^+ ion heat flow of parallel energy.

bi-Maxwellian model, the associated parallel heat flow (solid line) is higher than in the bi-Maxwellian solution (dotted line). Actually, around 2000 km the term $-m_s/2^{1/3}(q_s^{\parallel}/\rho_s)^{4/3}\partial n_s/\partial r$ is of the same order as the term $3n_s{k_B}^2T_{s\parallel}/m_s\partial T_{s\parallel}/\partial r$, which is the classicaly associated term with the thermal conductivity law. Above this altitude, Figure 1 illustrates the importance of the gradient of density with respect to the gradient of temperature in the evaluation of the parallel heat flow. For the perpendicular heat flow $q^{\perp}$ both models display a similar solution, with a slightly smaller generalized perpendicular heat flow (solid line) compared to the bi-Maxwellian perpendicular heat flow (dotted line).

As a consequence, the parallel temperature for the generalized model is equal to 6000 K at 4000 km in altitude, whereas the bi-Maxwellian model predicts a value of 8000 K at the same altitude. The perpendicular temperature is nearly the same for both solutions. The difference between the behavior of the parallel temperatures in both solutions could be explained by the gradient of the parallel and perpendicular heat flow with respect to the altitude. Indeed, in (3) an important contribution to the increase of parallel temperature is above 2000 km: $-1/(n_{H^+}k_B)\partial q_{H^+}^{\parallel}/\partial r$. For the perpendicular temperature equation (equation 4) this corresponds to $-1/(n_{H^+}k_B)\partial q_{H^+}^{\perp}/\partial r$. From Figure 1 it is obvious that the decrease of the parallel heat flow is smaller for the generalized solution than for the bi-Maxwellian solution. The gradient of the parallel heat flow in the generalized solution then generates a smaller increase of the parallel temperature. Another explanation for this discrepancy in the behavior of the parallel temperature appears in Figure 1b which shows significant difference between the H^+ velocity predicted by both models. The generalized model predicts a 15% higher velocity than the bi-Maxwellian model above 2500 km. The convection of energy is then higher, with the generalized model above 2500 km, which also contributes to an increase of the temperature smaller than in the bi-Maxwellian model. The H^+ velocity is increased by the new closure assumption because of a smaller temperature gradient in the generalized solution but also because of the thermal force [*Leblanc et al.*, 2000] associated with a higher parallel heat flow above 3000 km. As a consequence, the density is slightly smaller in the generalized solution because of the conservation of the H^+ flux. The sonic point in the generalized solution is at 3100 km, whereas the sonic point of the solution of the bi-Maxwellian is at 3300 km.

3.2. Role of the New Closure Assumption and Collisional Transfers

Another improvement provided by the generalized approach is the more accurate evaluation of the collisional transfers [*Leblanc et al.*, 2000]. We compare the solution obtained with the generalized model associated with the *Chodura and Pohl* [1971] collisional transfers and the bi-Maxwellian solution of the section 3.1. Figures 2, 3, and 4 present the different profiles of the macroscopic parameters of the three charged species obtained by the resolution of the complete generalized model in solid lines (including *Chodura and Pohl* [1971] collisional contributions) and the bi-Maxwellian model (dotted lines). The electron density and velocity are derived from the ion densites and velocities with the assumptions of charge neutrality and zero current.

These profiles show that the results obtained with the generalized and bi-Maxwellian models are in good agreement with the observations. The H^+ density is 80 cm^{-3} at 2000 km (see Figure 2a) and 15 cm^{-3} at 4000 km. The O^+ density is 10,000 cm^{-3} at 2000 km and 1500 cm^{-3} at 4000 km (Figure 2d). The mean H^+ velocity value is 2 km s^{-1} at 2000 km and 7.5 km s^{-1} at 4000 km, whereas the mean O^+ velocity is always $<$0.4 km s^{-1} (Figure 2c). The sonic point is at 3200 km for the H^+ ions, while because of the boundary condition imposed on the velocity, the O^+ ions are always subsonic. The ion temperatures (Figure 3) evolve in a range 2000-5000 K with a maximum at 1500 km for the O^+ temperatures (Figures 3b and 3d) and the perpendicular H^+ temperature (Figure 3a), whereas the parallel H^+ temperature increases up to 5000 K at 4000 km (Figure 3d). The electron temperatures increase from 3000 K at 1000 km to 6000 K at 4000 km (Figures 3c and 3f). The heat flow (Figure 4) is slightly negative below 800 km and always positive for the H^+ ions above this altitude (Figures 4a and 4d). It is first negative and then positive from 1500 to 4000 km for the O^+ ions (Figures 4b and 4e) and always negative for the electrons (Figures 4c and 4f). The signs of these heat flows are then consistent with an upward flow associated with a decrease of the temperatures in the case of the electrons and the O^+ ions. Indeed, these two species have a low velocity compared to the thermal velocity and are then associated with a thermal conduction state dominated by the diffusion. For the H^+ ions the diffusion of these ions through a background of O^+ ions is associated with a nondiffusive thermal conduction.

The differences between the generalized and bi-Maxwellian solutions are especially significant for the H^+ ions. In Figures 2a and 2d the density profiles are very close for both approaches, but the density for the H^+ ions in the bi-Maxwellian solution is slightly smaller than in the generalized solution. This difference could be explained by the smaller value of the velocity predicted by the generalized model (between 5 and 10% less than the velocity of the solution of the bi-Maxwellian model) and the conservation of the flux from one model to the other (Figure 2c). Above 1000 km the profiles of the H^+ parallel and perpendicular temperatures diverge significantly (Figure 3). The generalized solution corresponds to a parallel temperature of 5000 K at 4000 km, whereas the bi-Maxwellian model is associated with a parallel temperature of 8000 K for the same altitude. The discrepancy for the perpendicular temperature be-

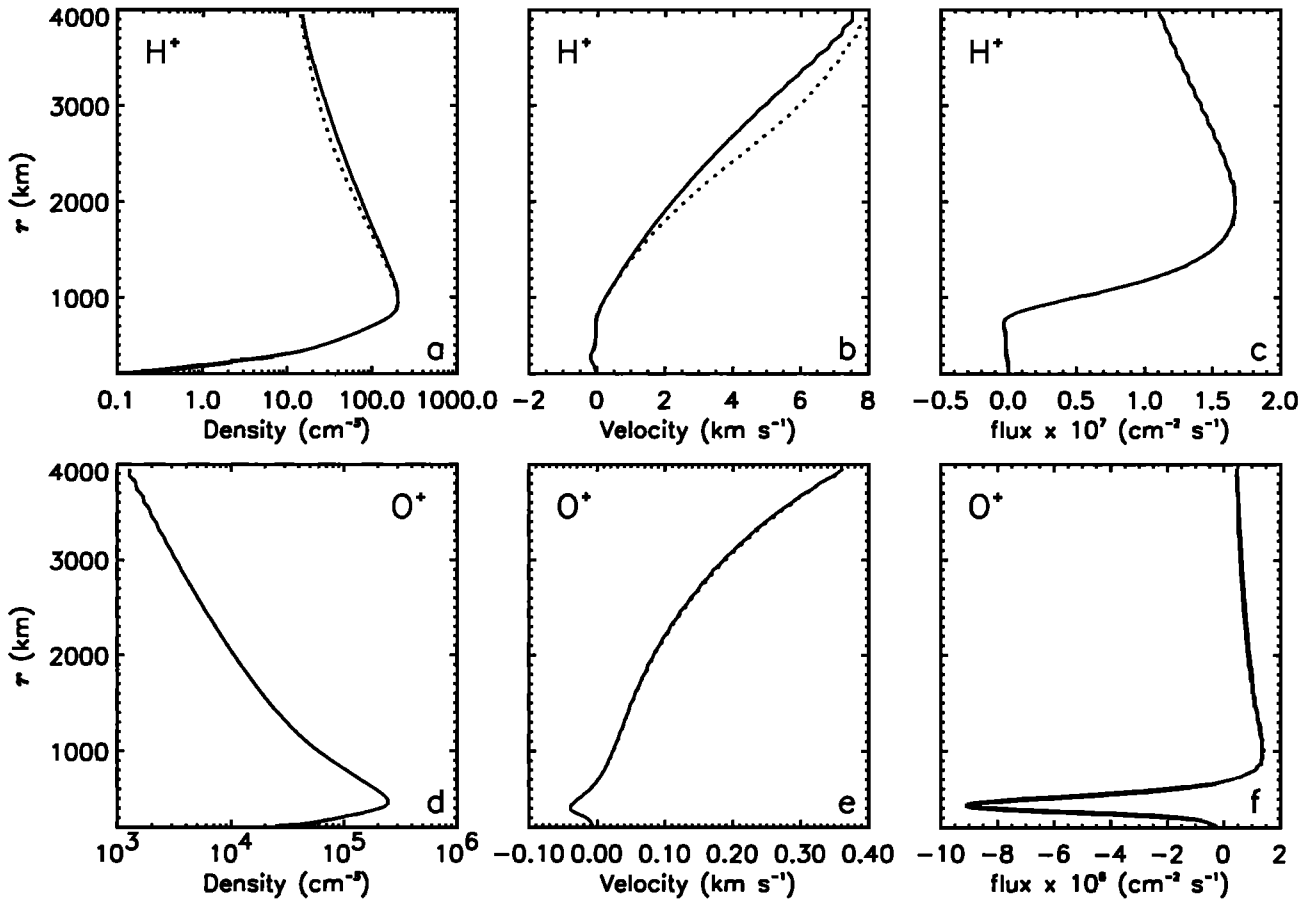

Figure 2. Solutions of the generalized model (solid line) and of the bi-Maxwellian model (dotted line): (a) H^+ ion density, (b) H^+ ion velocity, (c) H^+ ion flux, and (d) O^+ ion density, (e) O^+ ion velocity, (f) O^+ ion flux.

tween both models is of the same order: at 4000 km the generalized model predicts a 3000 K temperature, whereas the bi-Maxwellian solution is associated with a temperature of 5500 K. The temperature anisotropy is higher for the H^+ ions in the generalized solution. The main difference between the application of the section 3.1 and this application consists of a new expression of the energy collisional transfers. Indeed, there is no friction contribution in the collisional perpendicular energy transfers of *Chodura and Pohl* [1971], whereas *Blelly and Schunk* [1993] introduced such a term in the perpendicular energy collisional transfer. The H^+/O^+ Coulomb collisions, which raise the H^+ perpendicular temperature for altitudes up to 3000 km by friction in the bi-Maxwellian model, do not contribute to the increase of the perpendicular temperature in the generalized model. In the same way, *Leblanc et al.* [2000] have shown that the H^+/O^+ parallel energy transfers associated with the bi-Maxwellian model are overestimated with respect to the generalized model and the *Chodura and Pohl* [1971] expressions. The increase of the H^+ parallel temperature is then naturally smaller in the generalized solution. In this application the velocity of the H^+ ions is smaller in the generalized solution than in the bi-Maxwellian solution, contrary to the conclusions of section 3.1. This is due to the smaller H^+ temperature in the generalized solution.

Figure 4 displays the profiles of the parallel and perpendicular heat flow for the three species and both models. The differences between the two solutions are close to those associated with the application of the section 3.1. However, we can notice two changes due to the new expressions of the energy transfer. For the perpendicular heat flow the generalized solution provides a lower value of the energy transfer than the solution of the previous section (Figure 1a). It should be caused by the smaller gradient of perpendicular temperature in this solution. Indeed, the perpendicular temperature increases from 2×10^5 K to 5.5×10^5 K with the altitudes in the solution presented in section 3.1, whereas it is almost constant above 1000 km in the solution presented in this section. On the contrary, the parallel heat flow is higher in this application than in the solution of section 3.1 despite a smaller parallel temperature (Figure 1e). Indeed, the parallel temperature is equal to 5×10^5 at 4000 km for the solution of this section, whereas the H^+ temperature in section 3.1 is equal to 6×10^5 K at 4000 km. It is compensated by the decrease of the thermal convection in comparison with Figure 1 because of a smaller velocity in the generalized solution at higher

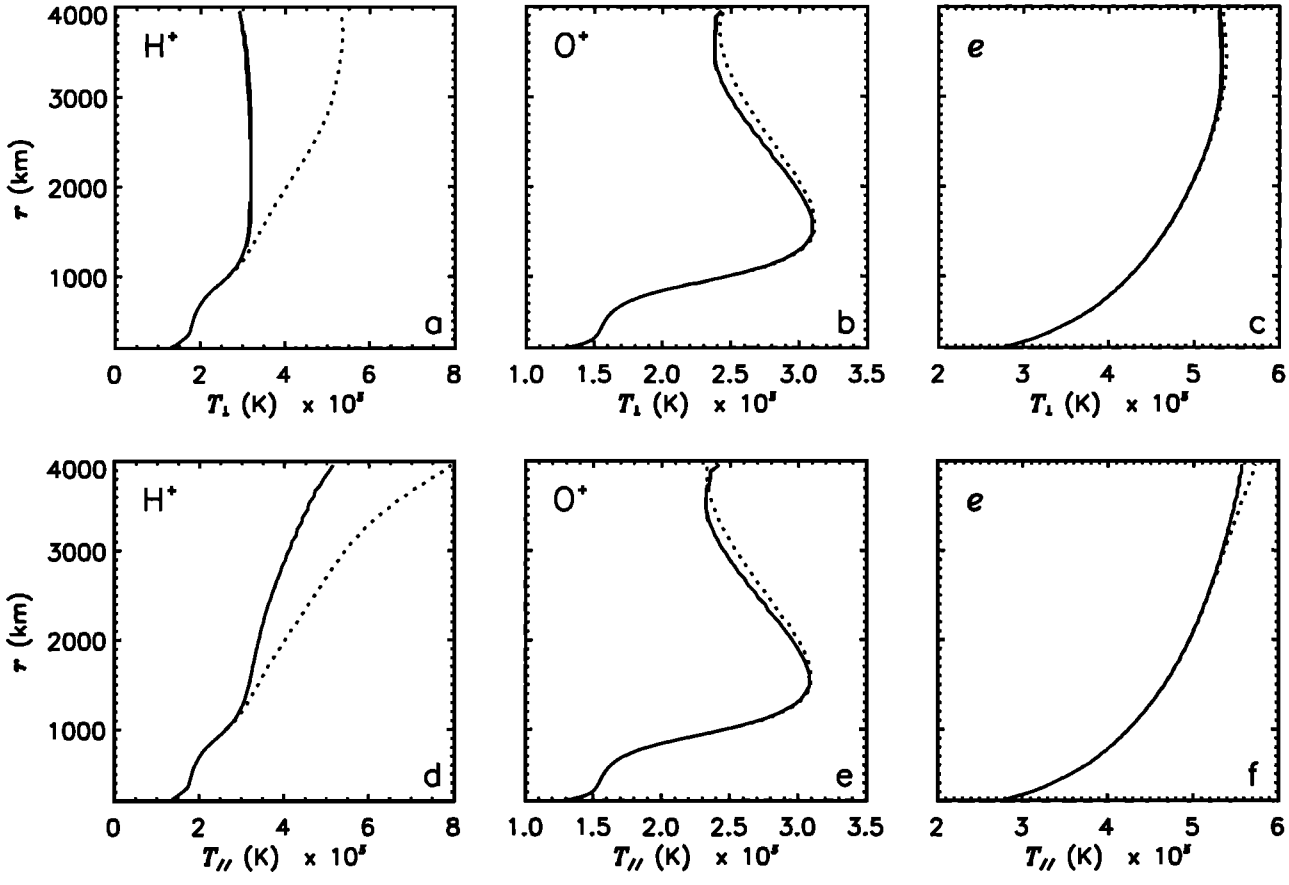

Figure 3. Solutions of the generalized model (solid line) and of the bi-Maxwellian model (dotted line): (a) H^+ ion perpendicular temperature, (b) O^+ ion perpendicular temperature, (c) electron perpendicular temperature, and (d) H^+ ion parallel temperature, (e) O^+ ion parallel temperature, (f) electron parallel temperature.

altitudes. Moreover, as we underlined in section 3.1, the role of the gradient of density in (5) is important above 2000 km. We here remark that because of the lower value of $T_{H^+\parallel}$ compared to the solution displayed in Figure 1, the importance of the gradient of density is increased with respect to the term proportional to the gradient of temperature.

The relative velocity between the H^+ ions and the O^+ ions and between the H^+ ions and the electrons, normalized by the thermal velocity $v_{th_{st}}$ associated with the two species ($v_{th_{st}} = (v_{th_s}^2 + v_{th_t}^2)^{1/2}$) is displayed in Figure 5a. It corresponds to a validity criterion for the construction of the collisional transfers [*Leblanc and Hubert*, 1999]. Figure 5a indicates that the assumption of a low value of the relative velocity in the semilinear assumption [*Leblanc et al.*, 2000] is always valid for the interaction between H^+ and electrons but is not valid for the interaction between H^+ and O^+. It implies that the collisional transfer expressions of the model of *Blelly and Schunk* [1993] are not well adapted, whereas the expressions we used in the generalized model and deduced from *Chodura and Pohl* [1971] are better suited to this application.

Leblanc and Hubert [1997, 1998, 1999] underlined the importance of the normalized parallel and perpendicular heat flow in the evaluation of the validity of the multimoment approaches. Let us recall that the normalized parallel heat flow of the s species is defined as the heat flow of parallel energy $q_s^{\parallel}$ normalized by the parallel free streaming heat flow: $n_s m_s (k_B T_{s\parallel}/m_s)^{3/2}$. The normalized perpendicular heat flow is normalized by the perpendicular free streaming heat flow: $n_s m_s (k_B T_{s\perp}/m_s)^{3/2}$. Figures 5b and 5c display such parameters with respect to the altitudes for the generalized (solid line) and bi-Maxwellian (dotted line) approaches. The H^+ parallel and perpendicular normalized heat flows reach a maximum near the sonic point in the bi-Maxwellian solution. They seem to tend to a limit in the generalized solution for the H^+ ions. *Leblanc and Hubert* [1997, 1998, 1999] established that the closure assumption of the multimoment approach is not valid when the normalized parallel and perpendicular heat flows exceed a threshold. For higher values of these parameters, negative values of the distribution function appear. Figure 6 displays the profiles of the H^+ velocity distribution function associated with the

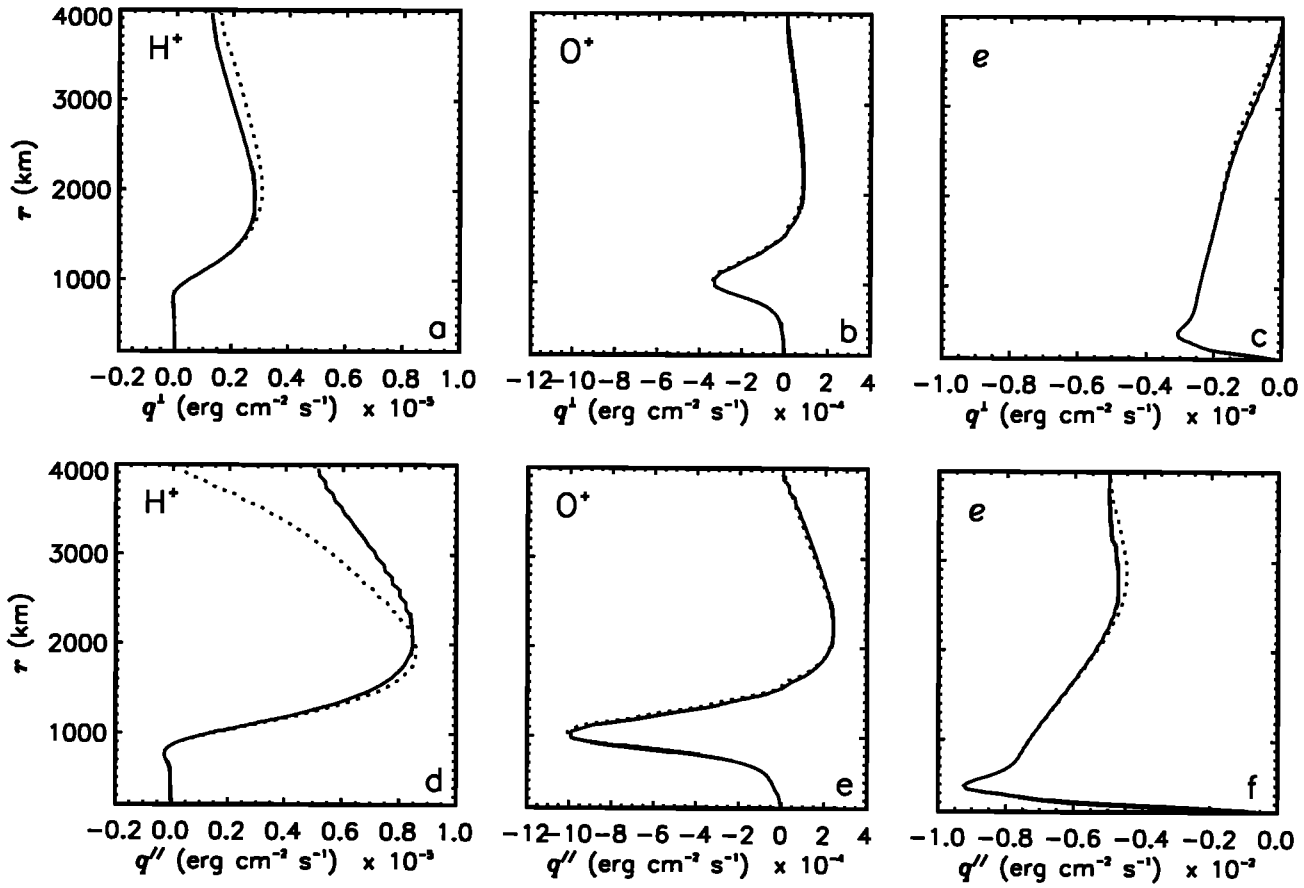

Figure 4. Solutions of the generalized model (solid line) and of the bi-Maxwellian model (dotted line): (a) H^+ ion heat flow of perpendicular energy, (b) O^+ ion heat flow of perpendicular energy, (c) electron heat flow of perpendicular energy, and (d) H^+ ion heat flow of parallel energy, (e) O^+ ion heat flow of parallel energy, (f) electron heat flow of parallel energy.

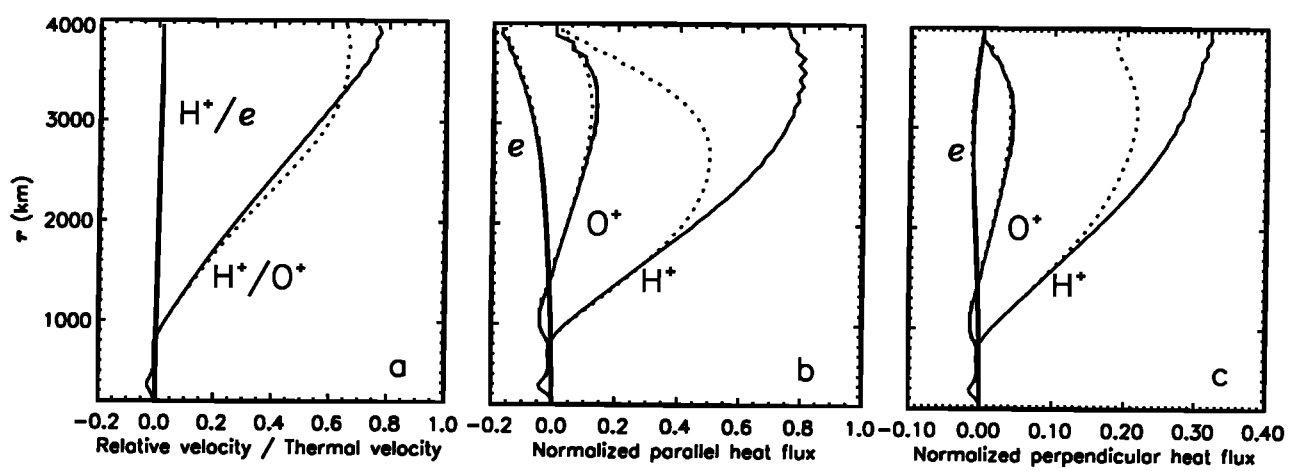

Figure 5. (a) Normalized relative velocity between the H^+ ions and the electrons and the H^+ and O^+ ions in function of the altitudes, (b) Normalized parallel heat flow for the electrons, and the H^+ and O^+ ions in function of the altitudes, (c) Normalized perpendicular heat flow for the electrons, and the H^+ and O^+ ions in function of the altitudes. The solid lines correspond to the solution of the generalized model, and the dotted lines correspond to the solution of the bi-Maxwellian model.

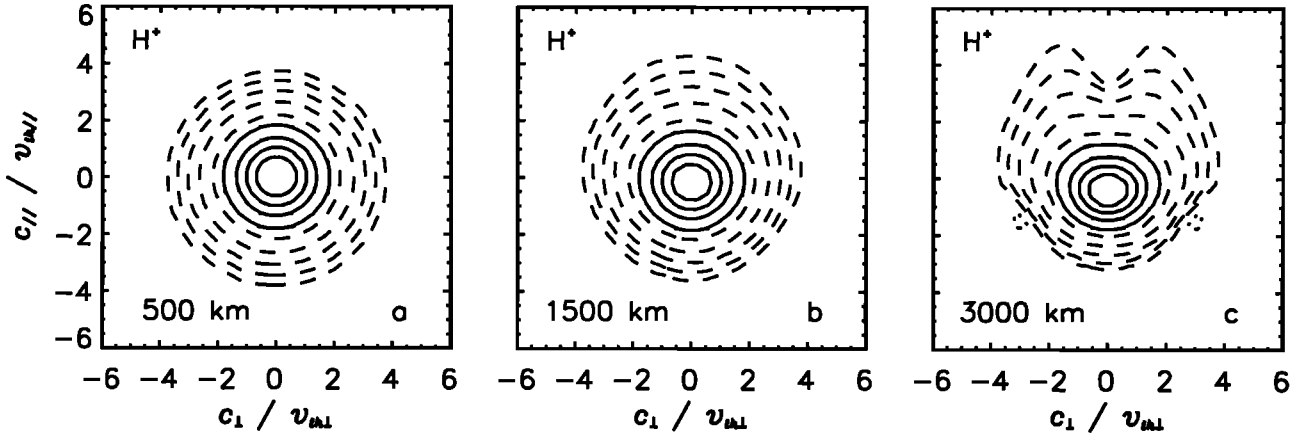

Figure 6. Two-dimensional representation of the velocity distribution function in the $(c_{\|}, c_{\perp})$ plane. These velocities are normalized by the parallel thermal velocity $V_{th\|}$ and the perpendicular thermal velocity $V_{th\perp}$. Contour lines correspond to fraction 0.8, 0.6, 0.4, and 0.2 (solid lines) and to 0.1, 0.032, 0.01, 0.0032, and 0.001 (dashed lines) of the maximum phase space density. The origin of the velocity space corresponds to the mean velocity. These functions have been obtained from the generalized model.

generalized model [*Leblanc and Hubert*, 1999] for three different altitudes. Figure 7 displays the same profiles but derived from the bi-Maxwellian approach. Close to a Maxwellian profile at 500 km, these profiles display at higher altitudes non-Maxwellian features. In Figures 6b and 7b, we have plotted the profiles of the H^+ distribution function at 3000 km in altitude. The profile of the velocity distribution function in Figure 6b is drastically deformed along the parallel direction for high positive values of the parallel velocity $c_{\|}/v_{th\|}$ (where $c_{\|}$ is the random velocity) and on the flank of the distribution for high negative values of $c_{\|}/v_{th\|}$. The core of the velocity distribution function develops an elongated profile in the perpendicular direction, whereas the complete (core plus halo) distribution is associated with a more pronounced asymmetry in the parallel direction. We determined that these deformations are due to the perpendicular normalized heat flow. In Figure 7 we plotted the same profile but for the bi-Maxwellian closure assumption. The distribution is associated with negative values for high negative parallel velocity. We determined that this property is due to the combining effect of relative high values of the normalized parallel and perpendicular heat flow. We have established that the bi-Maxwellian model provides significant negative values above 2000 km, whereas the generalized distribution function is still physically correct. Above 3000 km these characteristics are amplified. The profiles of the O^+ ion and electron distribution functions are always close to the Maxwellian profiles.

4. Discussion

Several different approaches have been applied to model the expansion of the terrestrial polar wind. In this section we compare the generalized solution pre-

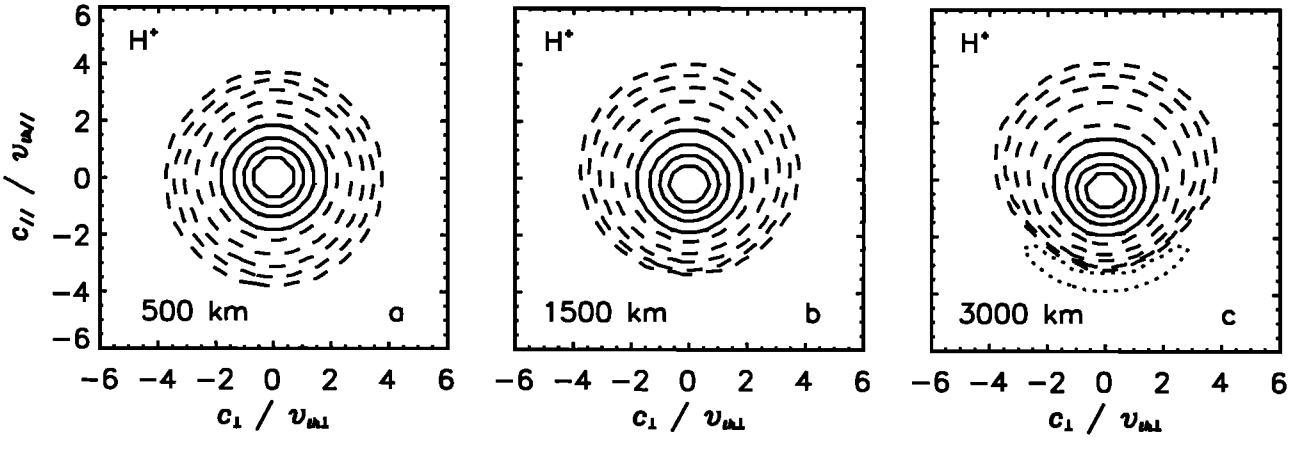

Figure 7. Velocity distribution functions derived from the bi-Maxwellian model for the same application as in Figure 6. The arrangement of the plots is as in Figure 6. The dotted line corresponds to a negative value of -0.001 of the maximum phase space density.

sented in the section 3.2 with solutions obtained by two different methods of resolution of the Fokker Planck equation in the context of the terrestrial polar wind.

The Monte Carlo method of solving the Fokker Planck equation is a very promising tool for tackling the expansion of particles from collision-dominated to collisionless regions. *Barghouthi et al.* [1993] have applied a Monte Carlo model to the expansion of H^+ ions through a background of O^+ ions at the thermodynamic and hydrostatic equilibrium state. In that paper the self-collisions between H^+ ions have been neglected, which is reasonable when the O^+ ion density dominates as is the case below 4000 km in altitude (Figure 2). The H^+/O^+ Coulomb collisions have been determined by using the Fokker Planck operator. The upward motion of the H^+ is due to the electrostatic force opposed to the gravitation force. The divergence of the magnetic field, similar to the configuration described in section 2, has been also included via the conservation of the total ion energy and of the first adiabatic invariant. Barghouthi et al. have determined a solution with a sonic point in the transition region between the collision-dominated region and the collisionless region. *Barakat et al.* [1995] provided the velocity distribution function profiles in the transition region. In this region a double-humped function appears to be aligned to the magnetic field direction, which then disappears to become what *Barghouthi et al.* [1993] call the kidney bean shape.

Lie-Svendsen and Rees [1996] have also determined an analytic solution of the Fokker Planck equation. They have considered the motion of H^+ and He^+ ions in a background of O^+ ions at the thermodynamic and hydrostatic equilibrium. From a collision-dominated region to upper altitudes (below 2500 km) they have considered Coulomb collisions between H^+/O^+ and He^+/O^+ ions. They have determined a sonic point at 2300 km in the transition region and have provided profiles of the distribution function between 2000 and 2500 km in altitude in good agreement with the results of *Barakat et al.* [1995].

These two approaches have obtained profiles of the H^+ velocity distribution, which evolve in the same way with respect to altitude. Close to a Maxwellian profile in the collision-dominated region, these profiles in the transition region are asymmetric in the parallel direction and associated with positive heat flow. In the collisionless region the profiles of the distribution function are associated with high temperature anisotropy with a larger perpendicular temperature. We could explain this evolution by the fact that the acceleration of the H^+ ions is due to the ambipolar electrostatic field, which is more important than the gravity field effect. The increase of energy due to the electrostatic field is independent of the original energy of the particle and is distributed between parallel and perpendicular energies. Since the electrostatic field is directed along the magnetic field direction, this increase of energy of the particle is mainly of parallel energy and is afterward distributed because of the conservation of the first adiabatic invariant. The main effect of the electrostatic field is to accelerate the H^+ ions with respect to the O^+ ions and to the electrons. However, the collisions between H^+ ions and other species generate a diffusion of the energy. At first this diffusion is mainly effective in the parallel direction, as long as the relative velocity between H^+ ions and O^+ ions is low. When this relative velocity increases, the diffusion turns to be more important in the perpendicular direction. Since the diffusion due to Coulomb collision decreases with high speed, the distribution function gets thinner in the parallel direction, mainly around the mean velocity of the species, i.e., around the core of the distribution. Then the parallel temperature and the thickness of the distribution along the magnetic field direction decrease when the perpendicular temperature increases in association with an increase in the thickness of the distribution in this direction.

The solution of section 3.2 provides similar evolution until the lower part of the transition region. Indeed, in the collision-dominated region (500 km in altitude; Figure 6a), the contour plots of the H^+ ions are close to a Maxwellian one. In the transition region (1500 km; Figure 6b), these contour plots then are asymmetric in the parallel direction and associated with a positive heat flow. The contour plots at 3000 km (Figure 6c) in the collisionless region are different. *Leblanc and Hubert* [1997] underlined that the generalized model could not reproduce the double-humped contour plot of *Barakat et al.* [1995]. Therefore we are not able to reproduce accurately the microscopic level of description in the upper part of the transition region. Let us stress that the two approaches display some differences: the Monte Carlo simulation does not take into account the interactions between H^+ and neutrals or the self-collisions H^+/H^+. By doing this the Monte Carlo simulations neglect several effects that make the H^+ distributions isotropic. However, above this region the core of the distribution function (Figure 6c) displays an elongated profile in the perpendicular direction, which is associated with a higher perpendicular temperature than the parallel temperature. Up to 4000 km in altitude the friction with the O^+ ions is still significant and, as explained in the section 3.2, generates an increase of the parallel temperature of the core plus halo distribution (Figures 1 and 3) contrary to the solution of *Lie-Svendsen and Rees* [1996] and *Barghouthi et al.* [1993]. The collisional energy transfers that we considered in the application of section 3.2 then generate an increase of the parallel temperature with respect to the perpendicular temperature, which is too high.

However, the correction of the *Blelly and Schunk* [1993] model by the collisional energy transfers of *Chodura and Pohl* [1971] generates a slight decrease of the perpendicular temperature contrary to the increase of the perpendicular temperature in the bi-Maxwellian solution (Figure 3). Moreover, *Leblanc et al.* [2000]

presented a comparison of the parallel and perpendicular energy collisional transfers obtained with the generalized expressions [*Leblanc et al.*, 2000] and with the *Chodura and Pohl* [1971] expressions. Above an altitude that depends mainly on the parallel and perpendicular heat flow values the parallel energy transfer is overestimated, and the perpendicular energy transfer is underestimated by the *Chodura and Pohl* [1971] expressions. We could then extrapolate that the exact generalized collisional transfers of energy would have generated a less important increase of the parallel temperature in better agreement with the results of *Lie-Svendsen and Rees* [1996] and *Barghouthi et al.* [1993]. As a consequence, the contour plots of the distribution function in the collisionless region would be more elongated in the perpendicular direction and closer to the typical profiles shown by *Lie-Svendsen and Rees* [1996] and *Barghouthi et al.* [1993].

5. Conclusion

The role of the suprathermal part of the velocity distribution function in the terrestrial polar wind has been described in several approaches [*Blelly and Schunk*, 1993; *Barakat et al.*, 1995; *Pierrard and Lemaire*, 1998]. However, none of these solutions allows an accurate, self-consistent description of its role in the transition between collision-dominated regions below 400 km and the collisionless region above 4000 km. In this paper we propose an original approach based on a multimoment multispecies method that has been developed in order to describe better the non-Maxwellian features of the species in this region.

This paper is the first application to the terrestrial polar wind of the generalized multimoment multispecies model [*Leblanc and Hubert*, 1997, 1998, *Leblanc et al.*, 2000]. We have compared this new multimoment multispecies 16-moment approach with the 16-moment bi-Maxwellian presented by *Blelly and Schunk* [1993] in a range of altitudes from the collision-dominated region to the collisionless region. However, because of the difficulty involved in using the new collisional transfers associated with the generalized model [*Leblanc et al.*, 2000] and because of the unacceptably long time needed to solve the associated set of transport equations, we have replaced in this application these contributions by an approximation deduced from the *Chodura and Pohl* [1971] expressions.

From this comparison we show the following.

1. When we only consider the effects of the new closure assumption on the higher-order velocity moment equations (equations (5) and (6)) without taking into account the changes in the collisional transfers, i.e., when we only study the effects of the new terms of transport in the equations for the heat flow we show that the generalized model predicts a higher velocity of the escaping supersonic particles (in our case it corresponds to the H^+ ions), that this acceleration is due to significant changes in the profiles of the temperature and of the heat flow, and that the new characteristics of these profiles are mainly due to a new term depending on the gradient of density that is involved in the description of the parallel heat flow.

2. When we also considered the new expressions of the energy collisional transfers approximated by the *Chodura and Pohl* [1971] expressions, the generalized model predicted a smaller velocity of the escaping supersonic particles compared to the previous application of the generalized model and a smaller increase of the parallel temperature and a decrease of the perpendicular temperature compared to the same application.

We also compared the generalized solution with the Monte Carlo model of *Barghouthi et al.* [1993] and of *Barakat et al.* [1995] and with the kinetic resolution of the Fokker Planck of *Lie-Svendsen and Rees* [1996]. We have noted differences in the temperature profiles that are reduced with respect to the difference between the bi-Maxwellian profiles and these approaches. The generalized model provides an approximation of the velocity distribution functions up to the collisionless region. These contour plots are close to the solutions determined by the Monte Carlo and kinetic approaches until the lower part of the transition region. In the upper part of the transition region the double-humped profiles predicted by the Monte Carlo and kinetic approaches are not reproduced by the generalized solution. In the collisionless region the kidney bean shape appears to be less pronounced in the generalized model because of the less important adiabatic cooling and perpendicular diffusion predicted by this model in its present status. Time reduction of the generalized collisional transfer calculations appears to be a necessary challenge as the collisional transfers would remedy these discrepancies. Such differences could also be explained by the effects of the H^+/H^+ self-collisions in the upper part of the transition region, which are taken into account in our model and not in the Monte Carlo or kinetic approaches.

The applications presented in this paper allow us to show the general good agreement of our model with measurements and previous models, in particular with the bi-Maxwellian model of *Blelly and Schunk* [1993]. However, they also show that this model is able to describe better the transition from collision-dominated regions to collisionless regions since it improves the agreement with the results obtained by kinetic models well adapted to the regions above 2000 km in altitude. These comparisons between generalized and bi-Maxwellian approaches provide a description of the nonthermal effects in the impulsion and energy transports during the expansion of the polar wind. These nonthermal effects are, in particular, suspected to play an important role in the high-altitude polar cap outflows escaping from Earth as stressed recently by *Moore et al.* [1997]. Future applications to the solar wind will allow the description, in a self-consistent way, of the expansion of this wind and also the underlining of the role of the nonthermal parts

of the electron and proton distribution functions, which are currently observed in the interplanetary medium. This model also provides a new and more accurate description of the heat flow in the transition region, which is of great importance in the solar corona according to recent papers [*Olsen and Leer*, 1996, 1999; *Li*, 1999]

Acknowledgments. Janet G. Luhmann thanks Abdallah Barakat and another referee for their assistance in evaluating this paper.

References

Abe, T., B. A. Whalen, A. W. Yau, R. E. Horita, S. Watanabe, and E. Sagawa, Exos D (Akebono) suprathermal mass spectrometer observations of the polar wind, *J. Geophys. Res., 98*, 11,191, 1993.

Banks, P. M., and T. E. Holzer, The polar wind, *J. Geophys. Res., 73*, 6846, 1968.

Barakat, A. R., I. A. Bargouthy, and R. W. Schunk, Double-humped H^+ velocity distribution in the polar wind, *Geophys. Res. Lett., 22*, 1857, 1995.

Barghouthi, I. A., A. R. Barakat, and R. W. Schunk, Monte Carlo study of the transition region in the polar wind: An improved collision model, *J. Geophys. Res., 98*, 17,583, 1993.

Blelly, P. L., and R. W. Schunk, A comparative study of the time dependent standard 8-, 13- and 16-moment transport formulations of the polar wind, *Ann. Geophys., 11*, 443, 1993.

Boris, J.P., Flux-corrected transport modules for generalized continuity equations, *NRL Memo. Rep. 3237*, Nav. Res. Lab., Washington, D.C., 1976.

Chandler, M. O., J. H. Waite Jr., and T. E. Moore, Observations of polar wind outflows, *J. Geophys. Res., 96*, 1421, 1991.

Chodura, R., and F. Pohl, Hydrodynamic equations for anisotropic plasmas in magnetic fields, II, Transport equations including collisions, *Plasma Phys., 13*, 645, 1971.

Demars, H. G., and R. W. Schunk, Transport equations for multispecies plasmas based on individual bi-Maxwellian distributions, *J. Phys. D Appl. Phys., 12*, 1501, 1979.

Ganguli, S. B., The polar wind, *Rev. of Geophys., 34*, 311, 1996.

Grad, H., Principles of the kinetic theory of gases, *Handb. Phys., 12*, 205, 1958.

Hedin, A. E., MSIS-86 thermospheric model, *J. Geophys. Res., 92*, 4649, 1987.

Leblanc, F., and D. Hubert, A generalized model for the proton expansion in astrophysical winds, I, The velocity distribution function representation, *Astrophys. J., 483*, 464, 1997.

Leblanc, F., and D. Hubert, A generalized model for the proton expansion in astrophysical winds, II, The associated set of transport equations, *Astrophys. J., 501*, 375, 1998.

Leblanc, F., and D. Hubert, A generalized multispecies model for the solar wind expansion, *AIP Conf. Proc., 471*, 389, 1999.

Leblanc, F., D. Hubert, and P.-L. Blelly, A generalized model for the proton expansion in astrophysical winds, III, The collisional terms and its properties, *Astrophys. J., 520*, in press, 2000.

Li, X., Proton temperature anisotropy in the fast solar wind: A 16-moment bi-Maxwellian model, *J. Geophys. Res., 104*, 19,773, 1999.

Lie-Svendsen, O., and M. H. Rees, An improved kinetic model for the polar outflow of a minor ion, *J. Geophys. Res., 101*, 2415, 1996.

Moore, T. E., et al., High-altitude observations of the polar wind, *Science, 277*, 349, 1997.

Olsen, E. L., and E. Leer, An eight-moment approximation two fluid model of the solar wind, *J. Geophys. Res., 101*, 15,591, 1996.

Olsen, E.L., and E. Leer, A study of solar wind acceleration based on gyro-tropic transport equations, *J. Geophys. Res., 104*, 9963, 1999.

Oyama, K.-I., and T. Abe, Morphology of electron temperature in the high latitude plasmaphere, *Adv. Space Res., 16* (1), 85, 1995.

Pierrard, V., and J. Lemaire, A collisional kinetic model of the polar wind, *J. Geophys. Res., 103*, 11,701, 1998.

Press, W. H., B. P. Flannery, S. A. Teukolsky, and W. T. Vetterling, *Numerical Recipes: The Art of Scientific Computing*, Cambridge Univ. Press, New York, 1989.

P.-L. Blelly, CESR, CNRS/UPS, 9, Avenue du Colonel Roche, 31028 Toulouse Cedex, France. (pierre-louis.blelly@cesr.fr)

D. Hubert, Département de Recherche Spatiale, CNRS URA 264, Observatoire de Paris, 92195 Meudon Cedex, France. (daniel.hubert@obspm.fr)

F. Leblanc, Department of Astronomy, University of Virginia, P.O. Box 3818, Charlottesville, VA 22903-0818. (fl3x@virginia.edu)

(Received June 8, 1999; revised October 13, 1999; accepted November 1, 1999.)